

# Compressive sensing reconstruction for compressible signal based on projection replacement

Zan Chen<sup>1</sup> · Xingsong Hou<sup>1</sup> · Chen Gong<sup>2</sup> ·  
Xueming Qian<sup>1</sup>

Received: 24 September 2014 / Revised: 10 December 2014 / Accepted: 19 March 2015/  
Published online: 10 April 2015  
© Springer Science+Business Media New York 2015

**Abstract** Compressive sensing can reconstruct compressible or sparse signal at the under-sampling rate. However small coefficients of the compressible signal with large number but low energy are hard to be reconstructed, while also infect the accuracy of the big coefficients. In this reason, for the compressive sensing algorithms such as orthogonal match pursuit (OMP) and tree-structured wavelet compressive sensing (TSW-CS), an assumed error is in the measurement model, which makes the reconstructed results not satisfy the original measurement model. Aiming at this problem, we propose the projection replacement (PR) algorithm by building the measurement space and its orthogonal complement space with singular value decomposition, and replacing the projection in measurement space of the reconstructed result with the pseudo-inverse one. The proposed PR algorithm eliminates the hypothetic measurement error in OMP and TSW-CS reconstructed model, and it guarantees theoretically that the PR results have a smaller error. Its effectiveness is verified experimentally with OMP and TSW-CS. The proposed algorithm serves as a good reconstruction algorithm for the CS-based applications such as image coding, super-resolution, video retrieval etc.

**Keywords** Compressive sensing · Orthogonal projection · TSW-CS · OMP

---

✉ Xingsong Hou  
houxs-xjtu@qq.com

Zan Chen  
zancheng.1989@stu.xjtu.edu.cn

<sup>1</sup> School of Electronic and Information Engineering, Xi'an JiaoTong University, Xian, China

<sup>2</sup> School of Electronic and Information Engineering, University of Science and Technology of China, Hefei, China

## 1 Introduction

Compressive sensing (CS) is a new theory which can recover a sparse or compressible signal via a much smaller number of measurements than the dimension of the original signal [3]. CS reconstruction algorithm has been extensively investigated in the area of multimedia information process, such as image coding [2], super-resolution [10], video retrieval [13] etc. In [2], a Bayesian CS reconstruction method has been applied to multiple description coding (MDC). Such CS-based MDC enables traffic dispersion and can relieve net congestion [15]. In [4], super-resolution by greedy pursuits CS reconstruction method with highly coherent partial Fourier measurements is studied. In recent work [11], CS reconstruction algorithm has been used in 3-D reconstruction by transforming a low resolution depth map to a high resolution depth map. In [13], video retrieval problem is formulated as sparse reconstruction, and a Bayesian modeling and inference is utilized to tackle the video retrieval problem. CS reconstruction algorithm plays an important role in these CS-based applications.

Candés provides theoretical results that a sparse or compressible signal, with high probability, can be reconstructed optimally from random projections of this signal [1]. By acquiring a  $M \times 1$  dimensional vector  $y$  via linear measurements

$$y = \Phi\theta, \quad (1)$$

where  $\theta$ , a  $M \times 1$  dimensional vector, represents the coefficients in some transform domain such as Discrete Wavelet Transform (DWT) or Discrete Cosine Transform (DCT), and  $\Phi$ , a  $N \times M$  measurement matrix, models the sampling system, the CS reconstructed algorithms can get a sparse reconstructed result  $\tilde{\theta}$  close to the observed original signal  $\theta$ .

To find the sparse representation solution of a signal which has the fewest nonzero coefficients for (1) is a NP-hard problem. Various methods have been proposed to solve this problem, such as match pursuits (MP) [12], orthogonal matching pursuit (OMP) [14], tree-structured Bayesian compressive sensing implemented by variational Bayesian inference (TS-BCS-VB) [7] and tree-structured wavelet compressive sensing (TSW-CS) [6], which can be classified into greedy pursuit algorithms and Bayesian based algorithms. OMP and TSW-CS are the typical CS reconstruction algorithms that we expand in this paper.

Although the proposed algorithms have already achieved great success for sparse signal, the sparse assumption seems to be somewhat inconsistent with the real world signals, because most real signals are compressible rather than sparse. In other word, even if after an change of basis such as DWT, the transform coefficients still contain a large number of small coefficients. This inconsistent between assumption and reality leads to the problem that the CS reconstruction algorithms just reconstruct the big coefficients of the original signal approximately while ignore the small coefficients, which formulates (1) as

$$y = \Phi\tilde{\theta} + e, \quad (2)$$

where  $\tilde{\theta}$  represents the reconstructed approximate solution, and  $e$  is the measurement error led by the small coefficients.

One way to decrease  $e$  is to make  $\theta$  sparser by using a more adaptive transform such as directional lifting wavelet transform (DLWT) [8]. However, this method just decreases the  $e$ , but  $e$  still exists in DLWT domain. The other way assumes that  $e$  obeys some models. In greedy pursuit way [12, 14], it assumes K-sparsity in the original signal, and only K largest coefficients are reconstructed. Small coefficients are regarded directly as part of the noise

in CS measurement process. In Bayesian way [6, 7, 9],  $e$  is modeled by a Gaussian white noise with small variance.

In this work, we found a way to delimitate the measurement error  $e$  in (2). We propose an orthogonal projection replacement (PR) algorithm. We defined the measurement space  $c$ , and constructed its orthogonal complement space  $p$  with singular value decomposition (SVD) [5]. Then, the reconstructed results of the original reconstructed algorithms are divided into two parts: the orthogonal projection in space  $c$ , represented as  $\hat{\theta}_c$ , and the orthogonal projection in space  $p$ , represented as  $\hat{\theta}_p$ . By replacing  $\hat{\theta}_c$  with  $\theta_c$  (pseudo-inverse results [16]) in the original reconstructed result, we get a PR result  $\tilde{\theta}$ , which satisfies  $y = \Phi\tilde{\theta}$  and  $\|\theta - \tilde{\theta}\| \leq \|\theta - \hat{\theta}\|$ . Experimental results show the PR algorithm can improve the performance of OMP and TSW-CS. We also test PR algorithm with the different environmental noise level, which shows that it still works well in the low environmental noise.

The remainder of the paper is organized as follows. In Section 2, we discuss the measurement error of the compressible signal in the TSW-CS and OMP. In Section 3 we describe the proposed method, and prove its effectiveness. Example results are presented in Section 4, with different measurement number and noise level. Conclusions are provided in Section 5.

## 2 Compressible signal reconstruction

Assuming that the vector  $\theta$  [c.f. (1)] consists of  $K$  significant coefficients and  $M - K$  small coefficients. Then,  $\theta$  can be decomposed as  $\theta = \theta_K + \theta_e$ , where  $\theta_K$  represents the  $K$  significant coefficients and  $\theta_e$  represents the  $M - K$  small coefficients [6, 7]. Based on such decomposition, Eq. 1 can be rewritten as follows,

$$y = \Phi\theta_K + \Phi\theta_e = \Phi\theta_K + e. \quad (3)$$

Essentially, reconstruction  $\tilde{\theta}$  is the approximation of  $\theta_K$  at some under-sampling rate, and  $\theta_e$  serves as the interferences to the reconstruction of  $\theta_K$ .

TSW-CS is a model-based Bayesian algorithm based on hidden Markov tree (HMT) and Markov chain Monte Carlo (MCMC) inference [9]. In TSW-CS, each nonzero element of  $\theta_e$  is modeled by a zero-mean Gaussian noise with small variance, which leads to Gaussian assumption of the measurement error  $e$ . In this reason, TSW-CS can not delimitate the measure error  $e$ .

OMP is well-known for its greedy reconstruction, where in each step the dictionary vector that has the strongest correlation with the residual part of the signal is selected [14]. However, OMP can only reconstruct  $\theta_K$  in (3), which means OMP lost small coefficients  $\theta_e$ . In this reason, OMP can not delimitate the measure error  $e$ .

## 3 Projection replace algorithm

The proposed projection replacement algorithm is based on the singular value decomposition (SVD) of the measurement matrix  $\Phi$ . More specifically, we have the following decomposition,

$$\Phi = U\Delta V^T, \quad (4)$$

where  $U = [u_1, u_2, \dots, u_N] \in R^{N \times N}$  and  $V = [v_1, v_2, \dots, v_N, v_{N+1}, \dots, v_M] \in R^{M \times M}$ . In this section, we aim to construct the measurement space and the corresponding orthogonal complement space.

Let  $c = Span\{v_i\}_{i=1}^N$  be the measurement space, and  $p = Span\{v_i\}_{i=N+1}^M$  be the orthogonal complement space, where  $(v_{N+1}, v_{N+2}, \dots, v_M)$  are the orthogonal basis of the complement space. Let  $\Phi_{\perp} = [v_{N+1}, v_{N+2}, \dots, v_M]^T$  be the matrix forms of space p. We have that  $\Phi\Phi_{\perp}^T = 0$ .

Let  $\tilde{\theta}$  be the reconstructed vector with the traditional CS algorithm. It can be decomposed into the following,

$$\tilde{\theta} = \tilde{\theta}_c + \tilde{\theta}_p, \tag{5}$$

where  $\tilde{\theta}_c$  is the orthogonal projection of  $\tilde{\theta}$  in space c; and  $\tilde{\theta}_p$  is the orthogonal projection of  $\tilde{\theta}$  in space p.  $\tilde{\theta}_p$  can be calculated with

$$\tilde{\theta}_p = \Phi_{\perp}^T \Phi_{\perp} \tilde{\theta}. \tag{6}$$

Similarly, the original  $\theta$  can also be decomposed into the following two parts:

$$\theta = \theta_c + \theta_p, \tag{7}$$

where  $\theta_c$  and  $\theta_p$  are the orthogonal projection onto space c and space p, respectively. Note that we have the following  $\theta_c$  can still be achieved with the pseudo-inverse one, which is represented as

$$\theta_c = \Phi^T (\Phi\Phi^T)^{-1} y. \tag{8}$$

However,  $\theta_p$  can not be achieved, because it belongs to the null space of  $\Phi$ . In (5), replacing  $\tilde{\theta}_c$  with  $\theta_c$  and keeping  $\tilde{\theta}_p$ , we can obtain the following PR result  $\bar{\theta}$  from  $\tilde{\theta}$

$$\bar{\theta} = \theta_c + \tilde{\theta}_p. \tag{9}$$

From above all, the final result  $\bar{\theta}$  is

$$\bar{\theta} = \Phi^T (\Phi\Phi^T)^{-1} y + \Phi_{\perp}^T \Phi_{\perp} \tilde{\theta}. \tag{10}$$

The scheme of the proposed PR algorithm is depicted in Fig. 1. Firstly, a 2-dimensional sparse transform is applied to nature images. After the measurement, CS reconstructed algorithm is adopted to reconstruct the transform coefficients. Then PR algorithm is used to the

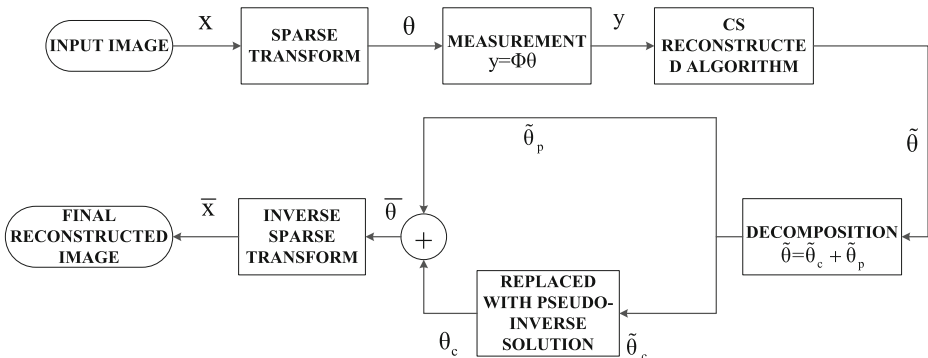


Fig. 1 Scheme of the PR algorithm

reconstructed results. Finally, reverse 2-dimensional sparse transform is performed to get the recovery of the original image.

The PR result  $\bar{\theta}$  satisfies:

$$y = \Phi\bar{\theta}, \tag{11}$$

and

$$\|\theta - \bar{\theta}\|_2^2 \leq \|\theta - \tilde{\theta}\|_2^2. \tag{12}$$

Substitute (10) into (11), we have the following

$$\Phi\bar{\theta} = \Phi\Phi^T(\Phi\Phi^T)^{-1}y + \Phi\Phi_{\perp}^T\Phi_{\perp}\tilde{\theta} = y.$$

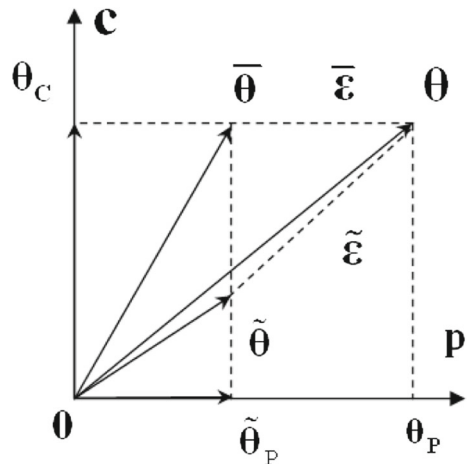
For (12), the error between  $\tilde{\theta}$  and  $\theta$  is given by

$$\begin{aligned} \|\theta - \tilde{\theta}\|_2^2 &= (\theta - \bar{\theta} + \bar{\theta} - \tilde{\theta})^T(\theta - \bar{\theta} + \bar{\theta} - \tilde{\theta}) \\ &= \|\theta - \bar{\theta}\|_2^2 + \|\bar{\theta} - \tilde{\theta}\|_2^2 + (\theta - \tilde{\theta})^T(\bar{\theta} - \tilde{\theta}) + (\bar{\theta} - \tilde{\theta})^T(\theta - \bar{\theta}) \\ &= \|\theta - \bar{\theta}\|_2^2 + \|\bar{\theta} - \tilde{\theta}\|_2^2 \\ &\quad + (\theta_c + \theta_p - \theta_c - \tilde{\theta}_p)^T(\theta_c + \tilde{\theta}_p - \tilde{\theta}_c - \tilde{\theta}_p) \\ &\quad + (\theta_c + \tilde{\theta}_p - \tilde{\theta}_c - \tilde{\theta}_p)^T(\theta_c + \theta_p - \theta_c - \tilde{\theta}_p) \\ &= \|\theta - \bar{\theta}\|_2^2 + \|\bar{\theta} - \tilde{\theta}\|_2^2 + (\theta_p - \tilde{\theta}_p)^T(\theta_c - \tilde{\theta}_c) \\ &\quad + (\theta_c - \tilde{\theta}_c)^T(\theta_p - \tilde{\theta}_p) \\ &= \|\theta - \bar{\theta}\|_2^2 + \|\bar{\theta} - \tilde{\theta}\|_2^2 \end{aligned}$$

It is seen that, given the original reconstructed error  $\|\theta - \tilde{\theta}\|_2^2$ , the reconstructed error  $\|\theta - \bar{\theta}\|_2^2$  decreases with  $\|\bar{\theta} - \tilde{\theta}\|_2^2$ ; and  $\|\theta - \bar{\theta}\|_2^2 \leq \|\theta - \tilde{\theta}\|_2^2$ .

Figure 2 provides an intuitive illustration of the projection relationship between the original  $\theta$ , the reconstructed  $\tilde{\theta}$  and the PR result  $\bar{\theta}$ . Note that  $\tilde{\varepsilon}$  is the original reconstructed error between  $\tilde{\theta}$  and  $\theta$ , and  $\bar{\varepsilon}$  is the replacement error between  $\bar{\theta}$  and  $\theta$ . It is obvious that  $\|\bar{\varepsilon}\|_2 \leq \|\tilde{\varepsilon}\|_2$ , which means that the PR result achieves a smaller reconstructed error.

**Fig. 2** The vertical axis represents the measurement space  $c$ , and the horizontal axis represents the orthogonal complement space  $p$



## 4 Experimental results

Let OMP-PR and TSW-CS-PR denote PR algorithms formulated in (10) based TSW-CS (<http://people.ee.duke.edu/lcarin/BCS.html>) and OMP (<http://sparselab.stanford.edu/>), respectively. Biorthogonal 9/7 filter (B9/7) is selected with 3-level wavelet transform and Gaussian random matrix is used as the measurement matrix. We test the performance gain of OMP-PR and TSW-CS-PR over baselines OMP and TSW-CS, respectively. To show the influence of the K-sparsity on the proposed method, we test OMP and OMP-PR in different K-sparsity levels. At last, we test the PR performance in low environmental noise.

### 4.1 Performance of the proposed method in different measurement numbers

We have evaluated the performance of the proposed CS PR algorithm on two different datasets, 50 test images from CVG-UGR (<http://decsai.ugr.es/cvg/dbimagenes/>) and 60 test images from USC-SIPI (<http://sipi.usc.edu/database/>), with respect to different measurement numbers. All standard test images are resized to  $128 \times 128$  by Photoshop. Nine image classes have been selected: Building, People, Satellite, Military and Miscellaneous 1 from dataset (<http://decsai.ugr.es/cvg/dbimagenes/>) and Texture, Aerials, Sequences and Miscellaneous 2 from dataset (<http://sipi.usc.edu/database/>). For TSW-CS, the 3-level Haar wavelet transform is replaced by the 3-level Biorthogonal 9/7 filter(B9/7) transform and other parameters are set to be default. For OMP, K-sparsity is chosen optimally with the best reconstructed quality. Table 1 shows the average Peak Signal-to-Noise Ratio (PSNR) of the TSW-CS, OMP and the associated PR results with 6000, 8000, 10000 and 12000 CS measurements in DWT domain and DLWT domain. We found that the PR algorithm works well for TSW-CS and OMP in both DWT domain and DLWT domain.

Figure 3 shows the representative images chosen from the classes of Building, People, Satellite, Military, Miscellaneous 1 for the dataset CVG-UGR, and Texture, Aerials, Sequence Miscellaneous 2 for the dataset USC-SIPI. The original images are shown in the first column in Fig. 3, and the reconstructed results from OMP, OMP-PR, TSW-CS and TSW-CS-PR are shown respectively from the second column to the fifth column. It is seen that OMP and TSW-CS algorithms incur some blurring effects, while OMP-PR and TSW-CS-PR algorithms present more details.

### 4.2 Performance of the OMP-PR with different K-sparse level

From Fig. 2 it is seen that the improvement of the PR algorithm relies on the relative distribution of  $\theta$  and  $\tilde{\theta}$  in space  $c$  and space  $p$ . To show this intuitively, we further show the reconstructed  $\tilde{\theta}$  and the PR result  $\hat{\theta}$  in Fig. 4a, with respect to relative error. In Fig. 4b, as the K-sparsity increases, the reconstructed error in space  $c$  always decreases, and thus the improvement of OMP-PR over the OMP decreases. From Fig. 4a we can also see that the reconstructed error in space  $p$  decreases and then increases after a turning point, which corresponds to the K-sparsity 1800. This means that the optimal performance of the OMP-PR is achieved for the K-sparsity 1800 since the error of OMP-PR is only limited in space  $p$ , while the optimal performance of OMP is achieved via minimizing the error in space  $c$  and space  $p$  jointly, at the K-sparsity 2400. Note that OMP-PR and OMP achieve the optimal performance for different K-sparsity. Similar results are observed for other images.

**Table 1** Mean PSNR results for each class in DLWT and DWT domain (dB)

Images	Algorithms	Number of measurements											
		6000			8000			10000			12000		
		DLWT	DWT	DWT	DLWT	DWT	DWT	DLWT	DWT	DWT	DLWT	DWT	DWT
CVG-UGR ( <a href="http://decsai.ugr.es/cv/dbrimages/">http://decsai.ugr.es/cv/dbrimages/</a> )	OMP	24.67	24.18	26.89	26.41	29.30	27.60	31.79	30.74				
	<b>OMP-PR</b>	25.70	25.15	27.92	27.51	30.32	29.80	33.31	32.87				
	TSW-CS	28.09	27.68	30.22	29.81	32.22	31.82	34.36	33.86				
	<b>TSW-CS-PR</b>	<b>28.53</b>	<b>28.12</b>	<b>30.91</b>	<b>30.53</b>	<b>33.33</b>	<b>32.94</b>	<b>36.22</b>	<b>35.76</b>				
People	OMP	26.31	25.56	28.80	28.21	31.61	29.32	34.43	33.09				
	<b>OMP-PR</b>	27.14	26.36	29.74	29.12	32.52	31.61	35.97	35.33				
	TSW-CS	30.07	29.36	32.44	31.93	34.81	34.27	37.11	36.68				
	<b>TSW-CS-PR</b>	<b>30.46</b>	<b>29.73</b>	<b>33.02</b>	<b>32.52</b>	<b>35.78</b>	<b>35.26</b>	<b>38.80</b>	<b>38.42</b>				
Satellite	OMP	23.49	23.09	24.15	24.13	25.67	25.05	27.44	26.84				
	<b>OMP-PR</b>	24.95	24.53	25.95	26.04	27.90	26.89	29.94	28.71				
	TSW-CS	26.13	25.88	27.30	27.05	28.47	28.15	29.74	29.48				
	<b>TSW-CS-PR</b>	<b>26.74</b>	<b>26.49</b>	<b>28.21</b>	<b>27.97</b>	<b>29.83</b>	<b>29.53</b>	<b>31.84</b>	<b>31.62</b>				
Military	OMP	27.78	27.57	29.11	29.02	30.84	30.13	32.63	32.30				
	<b>OMP-PR</b>	29.04	28.82	30.70	30.56	32.61	32.19	34.78	34.28				
	TSW-CS	30.73	30.69	32.14	32.12	33.42	33.47	34.76	34.74				
	<b>TSW-CS-PR</b>	<b>31.34</b>	<b>31.28</b>	<b>33.06</b>	<b>33.05</b>	<b>34.79</b>	<b>34.85</b>	<b>36.92</b>	<b>36.91</b>				
Miscellaneous 1	OMP	26.85	26.29	29.37	28.99	32.35	29.99	34.92	33.82				
	<b>OMP-PR</b>	27.71	27.18	30.43	29.96	33.40	32.26	36.59	36.05				
	TSW-CS	30.72	30.47	33.19	32.85	35.46	35.21	37.61	37.34				
	<b>TSW-CS-PR</b>	<b>31.12</b>	<b>30.86</b>	<b>33.81</b>	<b>33.47</b>	<b>36.49</b>	<b>36.28</b>	<b>39.43</b>	<b>39.19</b>				

**Table 1** (continued)

Images	Algorithms	Number of measurements								
		6000		8000		10000		12000		
		DLWT	DWT	DLWT	DWT	DLWT	DWT	DLWT	DWT	
USC-SIPI ( <a href="http://sipi.usc.edu/database/">http://sipi.usc.edu/database/</a> )	Texture	OMP	20.90	20.84	22.09	21.85	23.89	23.67	26.27	26.12
		<b>OMP-PR</b>	22.41	22.36	23.77	23.67	25.60	25.42	28.32	28.20
		TSW-CS	23.82	23.62	25.43	25.24	27.48	27.19	29.44	29.31
		OMP	25.07	24.58	26.29	25.91	27.96	27.59	29.93	29.52
Aerials		<b>OMP-PR</b>	26.48	25.96	28.03	27.60	29.85	29.46	32.21	31.74
		TSW-CS	28.11	27.76	29.61	29.26	31.11	30.81	32.69	32.49
		<b>TSW-CS-PR</b>	<b>28.69</b>	<b>28.33</b>	<b>30.44</b>	<b>30.08</b>	<b>32.33</b>	<b>32.03</b>	<b>34.61</b>	<b>34.36</b>
		OMP	29.61	28.86	32.26	31.57	34.98	34.43	37.47	36.92
Sequence		<b>OMP-PR</b>	30.50	29.71	33.25	32.54	36.07	35.51	39.20	38.65
		TSW-CS	33.30	32.72	35.93	35.16	37.97	37.45	39.86	39.41
		<b>TSW-CS-PR</b>	<b>33.72</b>	<b>33.15</b>	<b>36.60</b>	<b>35.83</b>	<b>39.07</b>	<b>38.55</b>	<b>41.75</b>	<b>41.28</b>
		OMP	27.27	26.70	30.05	29.54	33.15	32.71	35.64	35.32
Miscellaneous 2		<b>OMP-PR</b>	28.12	27.57	31.13	30.60	34.42	33.96	37.51	37.19
		TSW-CS	31.33	30.85	33.94	33.68	36.17	35.94	38.02	37.90
		<b>TSW-CS-PR</b>	<b>31.78</b>	<b>31.28</b>	<b>34.68</b>	<b>34.36</b>	<b>37.38</b>	<b>37.12</b>	<b>40.10</b>	<b>39.93</b>
		<b>TSW-CS-PR</b>	<b>24.39</b>	<b>24.24</b>	<b>26.26</b>	<b>26.09</b>	<b>28.69</b>	<b>28.44</b>	<b>31.30</b>	<b>31.21</b>

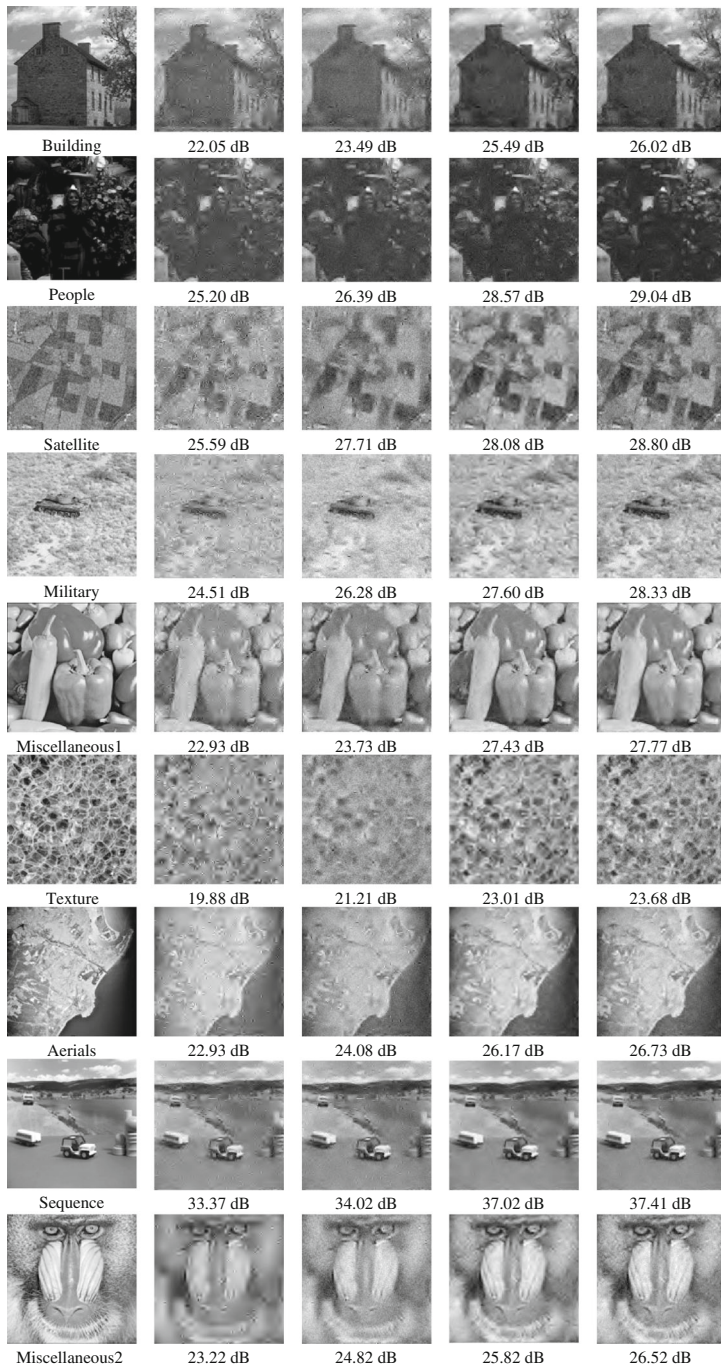


**Fig. 3** Nine images are respectively from Buildings, People, Satellite, Military, Miscellaneous 1, Texture, Aerials, Sequence and Miscellaneous 2. The original images and reconstructed results by OMP, OMP-PR, TSW-CS and TSW-CS-PR algorithms in DWT domain with 6000 measurement number are respectively shown from left to right

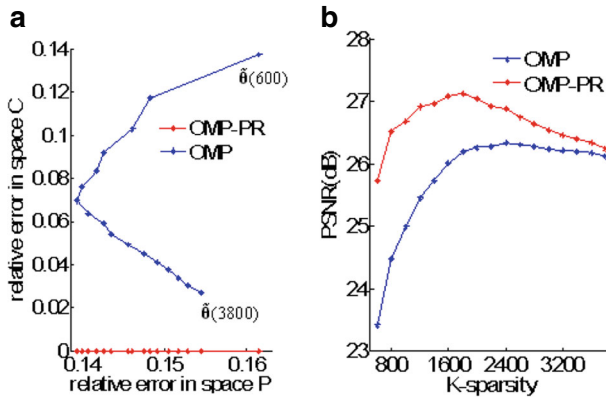


**Fig. 4** OMP and OMP-PR reconstructed results for  $128 \times 128$  Lena from K-sparsity 600 to 3800 at 0.5 sampling rate. K-sparsity step between two star-points is 200: (a) relative reconstructed error is in space c and space p, formulated as  $\frac{\|\theta_c - \hat{\theta}_c\|_2}{\|\theta\|_2}$  and  $\frac{\|\theta_p - \hat{\theta}_p\|_2}{\|\theta\|_2}$  respectively; (b) reconstructed PSNR for the corresponding K-sparsity

### 4.3 Performance in low environmental noise

Suppose there exists environmental noise in the measurement process, i.e., that (1) turns to  $y = \Phi\theta + n$ , where  $n$  obeys white Gaussian distribution  $N(0, \sigma^2)$ , where  $\sigma$  shows the

**Table 2** Results with different level noise in DWT domain (dB)

Images	Algorithms	Noise Level ( $\sigma$ )				
		0.018	0.01	0.006	0.003	
CVG-UGR ( <a href="http://decsai.ugr.es/cvg/dbimagenes/">http://decsai.ugr.es/cvg/dbimagenes/</a> )	Boat	OMP	24.49	24.61	24.63	24.61
		<b>OMP-PR</b>	25.88	26.17	26.25	26.25
		TSW-CS	28.34	28.78	28.89	29.04
		<b>TSW-CS-PR</b>	<b>28.63</b>	<b>29.25</b>	<b>29.43</b>	<b>29.53</b>
	Building	OMP	24.51	24.68	24.77	24.74
		<b>OMP-PR</b>	25.82	26.19	26.34	26.32
		TSW-CS	28.46	29.07	29.16	29.36
		<b>TSW-CS-PR</b>	<b>28.65</b>	<b>29.41</b>	<b>29.54</b>	<b>29.78</b>
Lena	OMP	24.79	24.98	24.99	25.02	
	<b>OMP-PR</b>	26.21	26.66	26.65	26.73	
	TSW-CS	29.27	29.93	30.19	30.25	
	<b>TSW-CS-PR</b>	<b>29.39</b>	<b>30.23</b>	<b>30.58</b>	<b>30.65</b>	
Peppers	OMP	24.36	24.28	24.30	24.47	
	<b>OMP-PR</b>	25.86	25.92	26.00	26.22	
	TSW-CS	29.42	30.24	30.45	30.50	
	<b>TSW-CS-PR</b>	<b>29.49</b>	<b>30.50</b>	<b>30.79</b>	<b>30.87</b>	

**Table 2** (continued)

Images	Algorithms	Noise Level ( $\sigma$ )				
		0.018	0.01	0.006	0.003	
Scenery	OMP	21.66	21.73	21.85	21.88	
	<b>OMP-PR</b>	23.10	23.25	23.42	23.47	
	TSW-CS	25.49	25.81	25.79	26.02	
	<b>TSW-CS-PR</b>	<b>25.93</b>	<b>26.32</b>	<b>26.31</b>	<b>26.54</b>	
USC-SPI ( <a href="http://sipi.usc.edu/database/">http://sipi.usc.edu/database/</a> )	Texture	OMP	20.81	20.74	20.80	20.87
		<b>OMP-PR</b>	22.71	22.86	22.90	22.91
		TSW-CS	24.59	24.71	24.74	24.78
		<b>TSW-CS-PR</b>	<b>25.27</b>	<b>25.45</b>	<b>25.53</b>	<b>25.55</b>
	Aerial	OMP	24.13	24.51	24.54	24.54
		<b>OMP-PR</b>	25.69	25.86	25.96	25.95
		TSW-CS	27.66	27.92	28.06	28.08
		<b>TSW-CS-PR</b>	<b>28.00</b>	<b>28.40</b>	<b>28.57</b>	<b>28.60</b>
	Sequence	OMP	33.18	34.83	35.91	35.98
		<b>OMP-PR</b>	33.32	35.53	36.67	36.87
		TSW-CS	35.94	38.09	39.37	40.20
		<b>TSW-CS-PR</b>	<b>34.81</b>	<b>37.80</b>	<b>39.53</b>	<b>40.65</b>
Miscellaneous	OMP	24.15	24.26	24.25	24.26	
	<b>OMP-PR</b>	26.01	26.20	26.31	26.29	
	TSW-CS	26.99	27.13	27.18	27.30	
	<b>TSW-CS-PR</b>	<b>27.53</b>	<b>27.78</b>	<b>27.90</b>	<b>28.02</b>	

environmental noise level. Nine images from CVG-UGR (<http://decsai.ugr.es/cvg/dbimagenes/>) and USC-SPI (<http://sipi.usc.edu/database/>) have been tested at 8000 measurement number in different noise level, as shown in Table 2. It is seen that the PR algorithm still performs well in low environmental noise.

## 5 Conclusions

In this work, we have proposed a CS improvement algorithm for compressible signal based on projection replacement. We construct the measurement space and its orthogonal complementary space, and decompose the traditional CS reconstruction into two parts, in the measurement space and in the orthogonal complementary space, where the part in measurement space is replaced with its pseudo-inverse. In this way, the reconstruction error is limited in the orthogonal complement space. Experimental results show the performance improvements of the PR algorithm. We have also shown that the PR algorithm works well in low environmental noise. The proposed method serves as an efficient reconstruction algorithm for CS-based applications such as image coding, super-resolution, video retrieval etc.

**Acknowledgments** This work was supported by National Natural Science Foundation of China (No.61373113) and the Fundamental Research for the Central University (No.xjj2012023).

## References

1. Cands EJ (2006) Compressive sampling. In: Proceedings of the international congress of mathematics, vol 3, pp 1433–1452
2. Deng CW, Lin WS, Lee B-S, Lau CT (2012) Robust image coding based upon compressive sensing. *IEEE Trans Multimed* 14(2):278–290
3. Donoho DL (2006) Compressive sensing. *IEEE Trans Inf Theory* 52(4):1289–1360
4. Fannjiang A, Liao W (2012) Super-resolution by compressive sensing algorithms. In: IEEE Proceeding Asilomar conference on signals, systems and computers, pp 411–415
5. Golub GH, Loan CFV (2013) Matrix computation, 4th edn. John Hopkins University Press, Maryland
6. He L, Carin L (2009) Exploiting structure in wavelet-based Bayesian compressive sensing. *IEEE Trans Signal Process* 57(9):3488–3497
7. He L, Chen H, Carin L (2010) Tree-structured compressive sensing with variational Bayesian analysis. *IEEE Signal Process Letters* 17(3):233–236
8. Hou XS, Yang J, Jiang GF, Qian XM (2013) Complex SAR image compression based on directional lifting wavelet transform with high clustering capability. *IEEE Trans Geosci Remote Sensing* 51(1):527–538
9. Ji S, Xue Y, Carin L (2008) Bayesian compressive sensing. *IEEE Trans Signal Process* 56(6):2346–2356
10. Kulkarni N, Nagesh P, Gowda R, Li BX (2011) Understanding compressive sensing and sparse representation-based super-resolution. *IEEE Trans Circuits Syst Video Technol* 22(5):778–789
11. Liu LW, Wang LH, Zhang M (2014) Depth map super-resolution based on joint dictionary learning. *Multimed Tools Appl*. doi:10.1007/s11042-014-2002-6
12. Mallat SG, Zhang Z (1993) Matching pursuits with time-frequency dictionaries. *IEEE Trans Signal Process* 41(3):3397–3415
13. Ruiz P, Babacan SD, Gao L, Li Z (2011) Video retrieval using sparse Bayesian reconstruction. In: 2011 IEEE international conference on multimedia and expo, pp 1–6
14. Tropp JA, Gilbert AC (2007) Signal recover from random measurement via orthogonal matching pursuit. *IEEE Trans Inf Theory* 53(12):4655–4666
15. Wang LJ, Wu XL, Shi GM (2008) A compressive sensing approach of multiple descriptions for network multimedia communication. In: Processing IEEE workshop multimedia signal process, vol 1, pp 445–449
16. Xu L, Liang Q (2010) Compressive sensing using singular value decomposition. In: Lecture notes in computer science, vol 6221, pp 338–342



**Zan Chen** received the B.S. degree from Xi'an Jiaotong University in 2012. Now he is pursuing his Ph.D. degree from Xi'an Jiaotong University, Xi'an, China. His research interest is image compressive sensing.



**Xingsong Hou** received the Ph.D. degree from Xi'an Jiaotong University, Xi'an, China, in 2005. Now, he is a Professor with the School of Electronics and Information Engineering, Xi'an Jiaotong University. His research interests include video/image coding, wavelet analysis, sparse representation, sparse representation and compressive sensing, and radar signal processing. During 2010–2011, he was a Visiting Scholar at Columbia University, New York, USA



**Chen Gong** received the B.S. degree in electrical engineering and mathematics (minor) from Shanghai Jiaotong University, Shanghai, China in 2005, and M.S. degree in electrical engineering from Tsinghua University, Beijing, China in 2008. He received the Ph.D degree in Electrical Engineering from Columbia University in May 2012. Now he is working in University of Science and Technology of China. His research interests are in the area of channel coding and modulation techniques for wireless communications and signal processing.



**Xueming Qian** received the B.S. and M.S. degrees from the Xi'an University of Technology, Xi'an, China, in 1999 and 2004, respectively, and the Ph.D. degree from Xi'an Jiaotong University, Xi'an, China, in 2008. He was awarded a Microsoft fellowship in 2006. From 1999 to 2001, he was an Assistant Engineer at Shanxi Daily. From 2008 until now, he has been a Faculty Member with the School of Electronics and Information Engineering, Xi'an Jiaotong University. He was a Visiting Scholar at Microsoft Research Asia from August 2010 to March 2011. His research interests include video/image analysis, indexing, and retrieval.